Title

Using Biomimetic Polymers in Place of Noncollagenous Proteins to Achieve Functional Remineralization of Dentin Tissues

Journal

ACS Biomaterials Science & Engineering, 3(12)

ISSN

2373-9878

Authors

Chien, Yung-Ching
Tao, Jinhui
Saeki, Kuniko
et al.

Publication Date

2017-12-11

DOI

10.1021/acsbiomaterials.7b00378

Peer reviewed

HHS Public Access

Author manuscript

ACS Biomater Sci Eng. Author manuscript.

Using biomimetic polymers in place of non-collagenous proteins to achieve functional remineralization of dentin tissues

Yung-Ching Chien[1,2], **Jinhui Tao**[1,3], **Kuniko Saeki**[2], **Alexander F. Chin**[2], **Jolene L. Lau**[1], **Chun-Long Chen**[1,3], **Ronald N. Zuckermann**[1], **Sally J. Marshall**[2], **Grayson W. Marshall**[2,*], and **James J. De Yoreo**[1,3,4,*]

[1]Molecular Foundry, Lawrence Berkeley National Laboratory, Berkeley, CA, 94720

[2]Department of Preventive and Restorative Dental Sciences, University of California, San Francisco, CA, 94143

[3]Physical Sciences Division, Pacific Northwest National Laboratory, Richland, WA 99352

[4]Department of Materials Science and Engineering, University of Washington, Seattle, WA, 98195

Abstract

In calcified tissues such as bones and teeth, mineralization is regulated by an extracellular matrix, which includes non-collagenous proteins (NCP). This natural process has been adapted or mimicked to restore tissues following physical damage or demineralization by using polyanionic acids in place of NCPs, but the remineralized tissues fail to fully recover their mechanical properties. Here we show that pre-treatment with certain amphiphilic peptoids, a class of peptide-like polymers consisting of N-substituted glycines that have defined monomer sequences, enhances ordering and mineralization of collagen and induces functional remineralization of dentin lesions *in vitro*. In the vicinity of dentin tubules, the newly formed apatite nano-crystals are co-aligned with the *c*-axis parallel to the tubular periphery and recovery of tissue ultrastructure is accompanied by development of high mechanical strength. The observed effects are highly sequence-dependent with alternating polar and non-polar groups leading to positive outcomes while diblock sequences have no effect. The observations suggest aromatic groups interact with the collagen while the hydrophilic side chains bind the mineralizing constituents and highlight the potential of synthetic sequence-defined biomimetic polymers to serve as NCP mimics in tissue remineralization.

Graphical abstract

*To whom correspondence should be addressed: james.deyoreo@pnnl.gov; GW.Marshall@ucsf.edu.

Supporting Information

The Supporting Information is available from the ACS Publications or from authors. Details of turbidity measurements from exemplar peptoids, Effect of peptoid pre-incubation, Reduced elastic modulus profile, AFM topographic image of remineralized dentin.

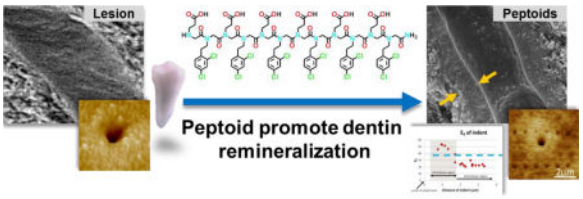

Keywords

Peptoids; dentin remineralization; in-situ AFM; Nanoindentation; TEM; SEM

Introduction

One of the salient features of biomineralization is that soluble proteins act in concert with an insoluble macromolecular scaffold to guide mineral formation[1]. In some cases, such as tooth enamel, the scaffold is sacrificial, while in others, including bone and dentin, it becomes an intricate part of the resulting composite and contributes to tissue function. One of the major challenges to successful repair of mineralized tissues is that an intimate spatial and temporal relationship between mineral, scaffold and soluble matrix is critical to achieving the biomineral-matrix ultrastructure necessary for that function, but that relationship is poorly understood and difficult to recreate. Repair of dental caries provide a case in point. As caries penetrate the outer enamel, which contains little or no organic matrix, it begins to demineralize the underlying dentin, which consists of hydroxyapatite (HAP) nanocrystals located within collagen fibrils (intrafibrillar) and between collagen fibrils (extrafibrillar)[2]. The bacterial attack is also accompanied by the release of bacterial and endogenous proteases in dentin, which leads to hydrolysis of the collagen scaffold as well as the NCPs[3]. When remineralization is attempted, the absence of NCPs inhibits the development of intrafibrillar HAP. Instead calcium phosphate precipitates on the lesion surface and mineralization does not support the individual collagen fibrils leading to low mechanical performance, e.g. low elastic modulus and hardness, of dentin[4–5].

Recently, some acellular, biomimetic remineralization approaches using polyanionic polymers to mimic the activity of NCPs' by regulating mineralization have shown promise for improved treatments[6–15]. For example, the polymer induced liquid precursor (PILP) process, which uses poly-L-aspartic acid (pAsp to aid the delivery of mineralizing constituents in the form of nanoclusters into collagen fibrils and form apatite after deposition of amorphous calcium phosphate[6–9], promotes intra-fibrillar mineralization critical to restoration of mechanical properties[4]. However, use of these polyanionic polymers only mimics biomineralization to a limited degree. Dentin, like other calcified collagenous tissues, contains numerous matrix-mineral interfaces[2] that are "bridged" and integrated by NCPs, which commonly have both conserved motifs that mediate matrix assembly[16–19] and anionic functional groups that interact with the highly charged mineral surfaces. Moreover, about 70% of the mineral content of dentin is extrafibrillar, while the amount of extrafibrillar mineral produced through the PILP process appears to be minor. Consequently, while polyanionic polymers can aid in forming intrafibrillar mineral, the extent, organization

and interaction of the HAP crystals and the collagen scaffold is inadequate for complete recovery of structure and function.

To improve this biomimetic strategy for functional remineralization, we began with the hypothesis that the function of NCPs is dependent upon their inherent sequence-specificity, which allows scaffold-directed and mineral directed motifs to be placed in an arrangement necessary to control both mineral formation and organization of the mineralizing matrix. To test this hypothesis, we then designed a small library of synthetic sequence-defined polymers presenting a mix of polar and non-polar side chains, with the expectation that the polar groups would act like the polyionic polymers in complexing the inorganic ions while the non-polar side-chains would mimic the phenylalanine (Phe), tyrosine (Tyr), and tryptophan (Trp) residues in NCP sequences that are believed to contribute matrix matrix interactions[20–23].

As our surrogate for NCPs we chose peptoids, which are N-substituted glycines that are able to form biomimetic structures across a wide range of length scales[24–26]. The peptoid backbone is identical to that of a peptide, but its side chains are attached to the nitrogen rather than the α-carbon, eliminating inter- or intra-chain hydrogen bonding and main-chain chirality, thus resulting in lower structural complexity and more facile synthesis. Peptoids also exhibit potent biological functionalities and are biocompatible[27–29]. In a recent study[30–31], dramatic modifications of $CaCO_3$ crystal growth rate and morphology by peptoids highlighted the potential of using these polymers for biomimetic approaches to controlling mineralization and remineralization. Here, we showed peptoids' potency to guide and modulate HAP mineralization on collagen substrates. Peptoids are potent and versatile for recapitulating ultrastructure and restoring the mechanical properties of tissues, useful for dentin remineralization given the fact that dentin doesn't undergo physiological remodeling and has limited self-regenerative ability.

Experimental Section

Peptoid synthesis

Peptoids were synthesized on polystyrene Rink amide resin (0.57 mmol/g) using either a Prelude or Aapptec automated peptide synthesizer and the solid-phase submonomer peptoid synthesis procedure, according to previously described methods[32–33]. The peptoids were cleaved from the resin using 95:2.5:2.5 TFA/H_2O/TIPS (v/v/v). The volatiles were removed using a Biotage V-10 evaporator to afford the crude peptoids, which were re dissolved in a mixture of acetonitrile and water (1:1, v/v) and purified by reverse phase HPLC using a C18 semi-preparative column (5 Mm, 250 mm × 21.2 mm, C18 Vydac column) with a flow rate of 15 mL/min. The collected fractions were concentrated and lyophilized to afford the purified peptoids as white, fluffy powders. Analytical HPLC analyses were performed on a 5 μm, 150 mm × 4.6 mm C18 Vydac column at 60 °C with a flow rate of 1.0 mL/min. HPLC traces were monitored at 214 nm.

We synthesized peptoids exhibiting two basic designs, one of which consisted of alternating hydrophobic and hydrophilic groups, while the other was based on a diblock sequence (Scheme 1). Each contained carboxylic acids (*N*-2-carboxyethylglycine) as hydrophilic

monomers and chloro- or dichloro substituted 2 phenylethyl units (*N*-(2-(4-chlorophenyl)ethylglycine *or N*-(2-(2,4-dichlorophenyl)ethylglycine) as hydrophobic monomers, and were differentiated through variations in the number and/or position of the hydrophilic and hydrophobic groups.

Turbidity measurements

To screen these candidate peptoids and assess their effectiveness in modulating calcium phosphate nucleation and growth in solution, we performed turbidity measurements commonly used in life science for drug compound solubility[34], bacterial or fungal growth studies[35], protein aggregation[36], antibody antigen interaction[37], and polymerization monitoring[38]. Turbidity test provides a high throughput, miniaturized, and parallel method to detect mineral formation, because two replicates of 12 peptoids at four different concentrations were assessed at once in a 96 well plate. By measuring the time required for mineralization to occur — i.e., the incubation time — as compared to control runs containing no polymer, the ability of peptoids to inhibit or promote nucleation was determined (Fig. 1 and Fig. S1).

Lyophilized peptoids (3.0×10^{-6} mol) were reconstituted in 1.5 mL Tris buffer saline (pH=7.4) in a glass vial, and brief ultra-sonication (< 1 min) was used as needed to facilitate dissolution. Reconstituted peptoids were further diluted in Tris buffered saline (TBS, pH=7.4) containing $[Ca^{2+}]$ = 13.5 mM, to make various micromolar concentrations (with exponential increase of base 2, e.g., 2, 4, 8, 16 μM) for testing. 15 μl of each calcium polymer mix was pipetted in each well and an equal volume of di-potassium phosphate solution at 6.3 mM was added, resulting in a calcium-to-phosphate ratio of 2.14. Two replicates of 12 peptoids were assessed in Corning 96-well UV-transparent microplate (Sigma Aldrich) in each turbidity test for up to 24 hours. The turbidity test uses a SpectraMax Plus 384 microplate reader to measure the absorbance of UV light (wavelength 320 nm and 600 nm, to ensure turbidity changes being recorded by either wavelength of light by software SoftMax Pro version 5). The absorbance of incident light increases with the nucleation and growth of calcium phosphate from solutions, i.e. the turbidity. The effect of each peptoid was compared to the control run with no addition of polymers (Figure 1).

Artificial caries preparation

Artificial carious lesions were prepared following methods that have been described previously in detail[39–40]. Non carious third molars were obtained from patients requiring extraction as part of their normal dental treatments following an approved protocol. After extraction the teeth were sterilized using gamma irradiation[41] and stored in DI water at 4° C until preparation. The crown was separated from the root and enamel was removed at the dentinoenamel junction (DEJ) using a slow-speed water cooled saw (Isomet, Buehler Ltd., Lake Bluff, IL) to obtain a dentin block (3×6×2.5 mm) exposing the dentin in the center of it. All occlusal surfaces were polished with diamond suspensions up to 0.25μm.

Two coats of acid resistant nail varnish (Revlon #270, New York, New York) were applied to all surfaces except a 3 mm × 3 mm window to expose dentin to simulate an occlusal natural carious lesion in a fissure. Each specimen (n = 6/group) was placed in a 50 ml

conical tube with 40 ml 0.05 M acetate buffer that contained 2.2 mM calcium and phosphate based on the recommendations by McIntyre et al.[42].

Demineralization was carried out for 66 hours based on a previously determined kinetic curve for the acetate buffer[40].

Remineralization of artificial caries

Peptoids that inhibited calcium phosphate nucleation and growth were used in experiments on mineralization of artificial human dentin lesions. Peptoid polymers were added at various micromolar concentrations to calcium chloride solution, or pre-incubated on dentin lesions before mineralization. An equal volume of di-potassium phosphate solution was added to the calcium-polymer mix, resulting in a calcium-to-phosphate ratio of 2.14. Solutions were prepared from reagent grade calcium chloride dihydrate ($CaCl_2 \cdot H_2O$), and potassium phosphate di-basic (K_2HPO_4) dissolved in Tris buffered saline (TBS, pH=7.4) and filtered to remove insoluble chemicals. Remineralization of dentin lesions with only peptoids was carried out for 14 days at 37°C with constant solution stirring.

To test whether peptoids counteracted or complemented poly-L-aspartic acid used in the PILP process, inhibitory peptoids were introduced 1) via pre-incubation on dentin lesions at fixed 2 μM for various times; 2) or mixing at 2 μM with poly-L-aspartic acid in calcium solution. Each specimen was then remineralized following a process similar to the PILP process for a period of 14 days at 37°C[39].

Atomic Force Microscopy

Monolayer collagen assembly—The collagen (brand name: Purecol) was obtained from Advance Biomatrix Corporation. This collagen solution contains 3.1 mg/mL of collagen (purified bovine Type I (97%) and Type III collagen (3%)) at pH 2.0, and was diluted in a phosphate buffer containing 300 mM KCl, 10 mM Na_2HPO_4 at pH7.40. The initial collagen concentration was fixed at 12 μg/mL in all cases to exclude the possibility of collagen assembly in liquid crystalline phase, which is known to occur in tissues and at high collagen concentrations (>20 mg/mL)[43–45]. The collagen solutions at desired concentration (12 μg/mL) were then applied onto a freshly cleaved muscovite mica disc (diameter 9.9 mm, Ted Pella, Inc.) and left for a 60-min incubation at pH 7.40, which was sufficiently long for collagen assembly onto the substrate.

AFM Imaging—All *in-situ* AFM images were captured in tapping mode at room temperature (23°C) with a NanoScope 8 atomic force microscope (Digital Instruments J scanner, Bruker) with hybrid probes consisting of silicon tips on silicon nitride cantilevers (SNL-10 triangular lever, k=0.35 N/m, tip radius <10 nm; resonance frequency 65 kHz in air; Bruker). The drive amplitude was about 20 nm (in fluid), and the signal-to-noise ratio was maintained above 10. The scanning speed was 1 Hz. The amplitude setpoint was carefully tuned to minimize the average loading force (~50 pN) during *in-situ* imaging.

The effects of various peptoid concentrations on calcium phosphate nucleation were investigated using *in situ* AFM on the freshly prepared monolayered collagen substrate in solutions at a fixed supersaturation, σ, of 3.34. The supersaturation is defined as $\sigma = \ln$

$((\alpha Ca^{2+})^5(\alpha PO_4^{3-})^3\ (\alpha OH^-)/Ksp)$, where α denotes the species activity, and *Ksp* denotes the equilibrium solubility constant at 25°C. This supersaturated (σ = 3.34) calcium phosphate solution was made by mixing 13.5 mM of $CaCl_2{\cdot}H_2O$ with 6.3 mM of K_2HPO_4 in equal volumes to achieve $[Ca^{2+}]$=6.75 mM and $[HPO_4^{2-}]$=3.15 mM. Preparation of each collagen substrate by assembly into a monolayer was performed immediately before the calcium phosphate nucleation experiments. The collagen substrate was briefly cleaned by flushing 1mL of deionized (≥18 MΩ) water to remove unbound collagen. Calcium and phosphate solutions were prepared immediately before use from reagent grade calcium chloride ($CaCl_2{\cdot}H_2O$), and potassium phosphate di-basic (K_2HPO_4) in Tris buffered saline (TBS, pH=7.4). Peptoids were introduced into the calcium solutions at various concentrations (100, 200, 500 nM and 2 μM).

Transmission electron microscopy

Transmission electron microscopy (TEM) of 70 nm ultra-thin sections prepared from 2 specimens per group were carried out to determine ultra-structures of remineralized lesion specimens and selected area electron diffraction (SAED) was used to identify the nature and crystallinity of the mineral formed by remineralization treatments. Sections from either artificial lesion or remineralization groups were embedded in Ultra Bed resin (Ultra-Bed Kit: a modification of Spurr's resin. Electron Microscopy Sciences, Hatfield, PA) after gradient dehydration in ethyl alcohol and then propylene oxide. Selected regions were trimmed, and ultrathin sections (70 nm) were cut in occlusal and sagittal planes with a diamond knife on an ultramicrotome (Reichert-Jung Ultracut E, Leica, Wetzlar, Germany). Ultrathin tissue sections were placed on Formvar™ copper grids and examined in a JEOL JEM 1400 TEM (JEOL Ltd, Tokyo, Japan) at an accelerating voltage of 120 kV. Images were recorded by CCD camera (Gatan Inc., Pleasanton, CA).

Scanning electron microscopy

Selected specimens (n = 2 per group) from the artificial lesion and remineralization groups were evaluated by scanning electron microscopy to characterize structural variations of remineralized dentin lesions. Specimens were coated with a 10–20 nm thick Au thin film using a sputter coater (Denton Vacuum Inc., Model # Desk II, Moorestown, NJ) and imaged using a Hitachi S-4300 field emission gun scanning electron microscope (Hitachi High Technologies America, Pleasanton, CA) at an accelerating voltage of 10 kV and using working distances larger than 12 mm, in general.

Elastic modulus measurements

Previous work has shown that measurement of mineral content alone does not always reflect the restoration of mechanical properties. Therefore we relied on nanoindentation to determine the reduced elastic modulus as described in prior studies in our laboratory[4–5, 39, 46]. An atomic force microscope (Nanoscope IIIA, Digital Instrument, Santa Barbara, CA) equipped with a Triboscope load-displacement transducer (Hysitron, Minneapolis, MN) and nanopositioner (nPoint, Middleton,WI) were used for nanomechanical property testing. The diamond indentation tips were calibrated with a fused silica standard in wet and dry conditions to measure E_R. The site specific reduced elastic modulus (E_R) was obtained with a 3 second trapezoidal loading curve as previously

described[47–48]. An AFM topographic image was acquired with the indentation tip along with the nanoindentation measurement to ensure the indentation was placed in the desired position, e.g. intertubular dentin only or peritubular dentin. In this study, in addition to examining cross-sections of lesions in wet conditions in the same manner as our previous works, we evaluated peptoid-induced mineral, because we observed distinct differences from the other remineralizing treatments. The elastic modulus of peptoid-induced mineral was evaluated in dry conditions to avoid degrading the deposited mineral.

Reduced elastic modulus of lesions from bottom to top (cross-section measurement)

Briefly, we did a series of nanoindentations along the cross sectioned lesions that extended from the most demineralized portion of the specimen through the transition zone and finished on the deeper normal dentin. This was done while the specimen is fully hydrated.

Cross sections of the lesion were prepared by removing excess moisture by blotting the dentin blocks containing the treated lesions prior to embedding them in room temperature curing epoxy (Epoxycure, Buehler, Lake Bluff, IL). The embedded blocks were cut with a slow speed saw under water (Buehler, Lake Bluff, IL) perpendicular to the treated occlusal surface to reveal the lesion profile. A thin slice obtained from the center of the specimen (~1200 μm) was glued onto the AFM specimen discs (Ted Pella, Redding, CA) with a small amount of cyanoacrylate (QX-4, MDS Products, Laguna Hills, CA), then polished through steps to a final polish with 0.25 μm diamond paste. Indentations in the lesion cross-section were made with a Berkovich tip (tip radius of about 100 nm) with a loading force varied over 200–500 μN to accommodate an E_R range from 0 to over 20 GPa.

Reduced elastic modulus of peritubular mineralization

Optical microscopy and AFM contact mode imaging were used on the cross-sectioned specimens to identify the depth and region with peritubular dentin modified by the peptoid-PILP treatment. The specimen was then carefully polished down to reveal the target depth in such way that the tubule orientation was perpendicular to the polished surface so that the indentation values would be least affected by underlying intertubular dentin. Site specific E_R values were obtained with a 3 second trapezoidal loading curve as cross-sectioned lesion in wet conditions. A sharp cube-corner tip (tip radius about 20nm) was employed for improved topographic imaging immediately after indentation. Indentation depths of 64 nm to 154 nm reflecting the differences in the material were obtained with a constant loading force of 300 μN. Dentin tubule occlusion induced by peptoids was imaged and evaluated by AFM: specimens without inhibitory peptoids were polished down to the same target depth as peptoid treated specimens that showed modification induced by the peptoids. Contact mode AFM in dry condition was used to capture images in 3 randomly selected areas (100 × 100 μm) of the specimens mineralized both with and without peptoid. The number of fully or partially occluded tubules and non-occluded tubules were counted to obtain the ratio of one to the other.

Results and Discussions

Screening peptoids using turbidity test

Peptoids with a di block structure (e.g., C792-3 or C792-5, Scheme 1) produced minor inhibition (C792-3) or a slight acceleration of nucleation (C792-5), displaying turbidity curves very similar to those obtained without the addition of peptoid (Fig. 1a and Fig. S1). To place that result in context, poly-L-aspartic acid used in the PILP process was found to strongly inhibit nucleation, producing a nearly flat curve (Fig. 1a and Fig. S2). In contrast to the diblock peptoids, those with hydrophobic and hydrophilic side groups alternately arranged along the backbone (e.g. CC81-3, Scheme 1) exhibited significant inhibition of calcium phosphate mineralization, with the incubation time increasing as the peptoid concentration increased (Fig. 1b and Fig. S2). In fact, no nucleation was detected for times exceeding 16 hours at a CC81-3 concentration of 8 μM (Fig. 1b). Inhibition of calcium phosphate nucleation is characteristic of natural NCPs and thus thought to be a key factor in collagen biomineralization[16–18]. We therefore chose inhibition or nucleation lag time as a criterion for selecting peptoids to be used in observations of collagen assembly and mineralization, as well as dentin remineralization.

Peptoids potential to improve biomimetic mineralization

We used *in situ* AFM to observe the assembly of collagen on mica into ordered matrices in which the collagen molecules are co aligned and exhibit the 67 nm periodicity of native collagen fibrils[49–50] (Fig. 2). After assembly in Tris buffer (Fig. 2a, left), the addition of inhibitory peptoids appeared to induce improved order (within 10 minutes) as measured by the degree of coverage and continuity of the gap and overlap zones, with higher peptoid concentration leading to further improvements and the creation of a nearly uniform and continuous sheet of ordered collagen (Compare Fig. 2a left vs right).

Mineralization of the ordered collagen matrices was then induced by injecting 2 mL calcium phosphate solution ($[Ca^{2+}]$ = 6.75 mM, $[HPO_4^{2-}]$ = 3.15 mM in tris buffer) into the AFM fluid cell, as described previously[51]. Under these conditions, the initial phase to form is amorphous calcium phosphate (ACP), which then transforms to octacalcium phosphate (OCP) and finally to HAP[51]. The results show that the addition of inhibitory peptoids to the collagen matrices impacts both the nucleation of ACP and its transformation to the crystalline phase (Fig. 2 b–e). For peptoid concentrations of 500 nM or less, both the incubation time for nucleation and the time to transformation were decreased, with the size of the effects growing as the peptoid concentration was increased (Fig. 2 b,c,e). However, at higher concentrations (2μM), both nucleation and transformation were inhibited (Fig. 2 d,e). The findings show that these peptoid designs also produce interactions with the inorganic constituents that impact the mineralization kinetics.

Dentin remineralization using peptoids as modulators

Given the ability of inhibitory peptoids to both impact collagen assembly and calcium phosphate mineralization, we tested their ability to promote remineralization of artificial human dentin lesions produced using acetic acid demineralization of human tooth as described previously[39] (Fig. 3a,b). In contrast to the results with either the peptoid-free

control or the diblock peptoid sequences, when dentin lesions were first incubated in solution containing inhibitory peptoids (30 μl of 2 mM peptoid solution until dry) prior to mineralization in peptoid-free solution (14 days in 40 ml of solution at 37°C with $[Ca^{2+}]$ = 4.5 mM, $[HPO_4^{2-}]$ = 2.1 mM in tris buffer with NaN_3 added as a biocide), a uniform calcium phosphate mineral layer formed on top of the lesion (Fig. 3b–d). This mineral layer closely contacted the underlying dentin lesion without gaps at the interfaces (Fig. 3c,d) forming a potentially protective layer on the demineralized lesion. Dentin tubules were also filled with calcium phosphate precipitates (Fig. 3e), and this further adhered the surface mineral layer to the dentin lesion.

Despite the encouraging results, the newly formed mineral layer did not permeate into the lesion matrix. Because previous work using the PILP process via introduction of pAsp to remineralize artificial dentin lesions led to extensive intrafibrillar mineralization in collagen matrices[9, 39, 52], we evaluated the potential synergistic effects of peptoids and pAsp for improving dentin remineralization. The incubation step was carried out with a mixture of inhibitory peptoid and pAsp solutions (2 mM peptoid and 100 μg/ml 27 kDa pAsp for times of 1 hour, 1day or 5 days) and remineralization was then performed in pAsp-containing solution (14 days in 40 ml of 100 μg/ml 27 kDa pAsp at 37°C with with $[Ca^{2+}]$ = 4.5 mM, $[HPO_4^{2-}]$ = 2.1 mM in tris buffer with NaN_3 added as a biocide).

The results show that the combination of pretreatment by inhibitory peptoids and mineralization via the PILP process produces remarkable recovery of dentin ultrastructure to the point that the remineralized lesion resembles normal dentin (Fig. 4a–d), with the extent of remineralization depending on incubation time (Fig. S3). In all cases for which dentin lesions (Fig. 4a,b) were pre-incubated with inhibitory peptoids, a collar of mineralization with substantial thickness was grown at the peritubular region of each dentin tubule akin to normal peritubular dentin (Fig. 4d) and the zone of mineralization extended into the lesion matrix. In contrast, PILP treatment alone induced mineralization in the collagen matrix but did not reestablish the peritubular dentin (Fig. 4c). Longer peptoid pre incubation promoted greater regrowth of peritubular dentin (See SI, Fig. S3). Mixing peptoids with pAsp in the PILP remineralization solution — i.e., no pre incubation — did not produce obvious peritubular mineralization (Fig. S3).

Close examination of the regrown peritubular minerals (Fig. 4e,f) showed that those formed through the PILP process after pretreatment with inhibitory peptoids were composed of lamellae of fine-crystalline apatite nano-crystals stacked along the tubular periphery (Fig. 4e) with better apparent alignment than those of normal dentin (Fig. 4f). Indeed, diffraction data showed that their *c* axes were mostly parallel to the long axis of the tubules (Fig. 4h). Thus treatment of the dentin lesions with inhibitory peptoids led to a high level of control over HAP nano-crystal formation and alignment.

Such distinctive ultrastructure of peritubular mineral layers is likely to produce exceptional mechanical properties. To determine the mechanical properties and evaluate the prospective application of these peptoid-induced peritubular mineral layers to clinical treatment, we performed AFM-based nanoindentation on the polished cross sectional surfaces of remineralized coronal dentin lesions. While normal peritubular dentin has a very constant

E_R of approximately 30 GPa[46, 53–55], about one third of depth of the lesion from the surface, the peritubular mineral of occluded tubules produced using pretreatment with inhibitory peptoids and PILP-based remineralization exhibited remarkably high values of reduced elastic modulus (E_R), ranging from 40–55 GPa (Fig. 4l). Examination of indentations obtained using an identical loading force for each measurement clearly shows the enhancement of the elastic modulus (Fig. 4k). The indentations on the hard peritubular mineral collar are much smaller and shallower than those in the remineralized intertubular dentin regardless of position, an outcome consistent with the exceptionally high values of E_R. Similar measurements on the intertubular dentin matrix show it also recovered more than 60% of its reduced elastic modulus (SI Fig. S4). The peritubular mineral growth induced by the inhibitory peptoid completely or partially filled at least 46% of tubules, much more structural recovery compared to lesions remineralized only with PILP process only (see SI, Fig. S5). The main reason for the larger E_R values is the higher mineral content that results from incubation of the dentin with peptoid solution, as seen in Fig. 4d. The alignment of the HAP platelets perpendicular to or at a high angle to the direction of the indentation force may also be a contributing factor.

The findings reported above show that the use of peptoids designed to interact with both the collagen matrix and mineralizing constituents enhances the in vitro assembly of collagen, impacts subsequent scaffold mineralization, and has a dramatic effect on remineralization of dentin lesions. The improvement of collagen assembly upon introduction of the inhibitory peptoid (compare Fig. 2a left vs. right) may be attributed to the interactions between the aromatic side groups of peptoids and the proline (Pro) and hydroxyproline (Hyp) residues of collagen monomers. Previous work showed that protons donated by Pro and Hyp residues can interact with acceptors such as electron rich aromatic groups, leading to CH$\cdots\pi$ interactions[20–23]. Other studies showed that π-π interactions between peptoids leads to their self-assembly into highly ordered structures[56]. Thus the high content of both Pro and Hyp on the surface of the collagen triple helix can be expected to promote extensive interactions with the phenethyl side groups of the peptoids and enhance the inter collagen interactions that promote co-alignment[50].

The impact on mineral formation is also understandable given the large number of carboxylic groups, which are well known to complex Ca^{2+} and comprise a large fraction of the amino acid side chains in natural biomineral associated proteins. The observed change from acceleration to inhibition of both nucleation and phase transformation as the concentration of inhibitory peptoids was increased, is reminiscent of the biomimetic activity reported for carboxyl-rich synthetic peptides[57], proteins extracted from natural biominerals[58], and even certain peptoids[31], all of which accelerated the growth of calcite crystals at nM concentrations, but inhibited growth at higher concentration, with the strongest inhibitors being the most potent accelerants. There as well, a mix of hydrophobic and hydrophilic groups was found to be important to achieve the effect and, though the mechanism remains unclear, ion binding by the carboxyl residues and hydrophobic interactions by the non-polar groups were implicated.

The high degree of nanocrystal alignment and packing in the peritubular region combined with the enhanced mechanical performance, which were absent when polyanionic polymers

alone were used[39], suggests that the integration of both functions, i.e., collagen binding and mineral ion complexation, into a single polymer is a critical design element. Moreover, the lack of any effect when diblock peptoids with the same constituent monomers are employed shows that polymer sequence is also a critical design element. Presumably the alternating hydrophobic-hydrophilic design maximizes the exposure of the phenethyl side groups to the collagen and of the carboxyl groups to the solvated ions when the peptoids and collagen helices are themselves coaligned, providing a ready template to promote co-alignment of the resulting HAP nanocrystals.

Conclusion

The peptoids chosen for this study were based on highly simplified designs with little of the compositional or structural complexity found in NCPs, yet they exhibit a remarkable level of control over dentin lesion remineralization. Given the large diversity of potential side chain chemistry (e.g., over 100 N substituted glycines are commercially available)[33] and the huge number of possible combinations of monomers, even for the short 12-mer designs used here, the results presented here highlight the tremendous potential offered by synthetic sequence defined polymers like peptoids as substitutes for NCPs in medical applications of tissue mineralization.

Supplementary Material

Refer to Web version on PubMed Central for supplementary material.

Acknowledgments

Tooth collection, preparation of dentin lesion specimens, remineralization experiments with peptoids and PolyASP were carried out at UCSF. In addition AFM based nanoindentations, additional optical, TEM and AFM imaging were also performed with all work at UCSF supported by NIH/NIDCR Grant R01 DE016849. Peptoid synthesis, AFM, and TEM were supported by and performed at the Molecular Foundry, which is operated by Lawrence Berkeley National Laboratory through support from the U.S. Department of Energy, Office of Science, Office of Basic Energy Sciences, Scientific User Facilities Division under Contract No. DEAC02-05CH11231. Y.C. Chien was partially supported by the Postdoctoral Fellowship from Fonds de la Recherche du Québec – Santé (FRQS, 2011–2013). Part of the research was performed at the Pacific Northwest National Laboratory (PNNL), a facility operated by Battelle for the U.S. Department of Energy.

References

1. Mann, S. Biomineralization: principles and concepts in bioinorganic materials chemistry. Oxford University Press; New York: 2001. p. xii198 p
2. Weiner, Sa, Wagner, HD. THE MATERIAL BONE: Structure-Mechanical Function Relations. Annu Rev Mater Sci. 1998; 28(1):271–298.
3. Buzalaf MA, Charone S, Tjaderhane L. Role of host-derived proteinases in dentine caries and erosion. Caries Res. 2015; 49(Suppl 1):30–7. [PubMed: 25871416]
4. Kinney JH, Habelitz S, Marshall SJ, Marshall GW. The importance of intrafibrillar mineralization of collagen on the mechanical properties of dentin. J Dent Res. 2003; 82(12):957–61. [PubMed: 14630894]
5. Bertassoni LE, Habelitz S, Kinney JH, Marshall SJ, Marshall GW Jr. Biomechanical perspective on the remineralization of dentin. Caries Res. 2009; 43(1):70–7.
6. Gower LB. Biomimetic model systems for investigating the amorphous precursor pathway and its role in biomineralization. Chem Rev. 2008; 108(11):4551–627.

7. Jee SS, Thula TT, Gower LB. Development of bone like composites via the polymer induced liquid precursor (PILP) process. Part 1: influence of polymer molecular weight. Acta Biomater. 2010; 6(9):3676–86.
8. Olszta MJ, Douglas EP, Gower LB. Scanning electron microscopic analysis of the mineralization of type I collagen via a polymer-induced liquid precursor (PILP) process. Calcif Tissue Int. 2003; 72(5):583–91.
9. Thula TT, Rodriguez DE, Lee MH, Pendi L, Podschun J, Gower LB. In vitro mineralization of dense collagen substrates: a biomimetic approach toward the development of bone-graft materials. Acta Biomater. 2011; 7(8):3158–69.
10. Gu L, Kim YK, Liu Y, Ryou H, Wimmer CE, Dai L, Arola DD, Looney SW, Pashley DH, Tay FR. Biomimetic analogs for collagen biomineralization. J Dent Res. 2011; 90(1):82–7.
11. Gu LS, Kim YK, Liu Y, Takahashi K, Arun S, Wimmer CE, Osorio R, Ling JQ, Looney SW, Pashley DH, Tay FR. Immobilization of a phosphonated analog of matrix phosphoproteins within cross-linked collagen as a templating mechanism for biomimetic mineralization. Acta Biomater. 2011; 7(1):268–77.
12. Kim YK, Gu LS, Bryan TE, Kim JR, Chen L, Liu Y, Yoon JC, Breschi L, Pashley DH, Tay FR. Mineralisation of reconstituted collagen using polyvinylphosphonic acid/polyacrylic acid templating matrix protein analogues in the presence of calcium, phosphate and hydroxyl ions. Biomaterials. 2010; 31(25):6618–27.
13. Niu LN, Zhang W, Pashley DH, Breschi L, Mao J, Chen JH, Tay FR. Biomimetic remineralization of dentin. Dent Mater. 2014; 30(1):77–96.
14. Tay FR, Pashley DH. Guided tissue remineralisation of partially demineralised human dentine. Biomaterials. 2008; 29(8):1127–37.
15. Zhang W, Luo XJ, Niu LN, Yang HY, Yiu CK, Wang TD, Zhou LQ, Mao J, Huang C, Pashley DH, Tay FR. Biomimetic Intrafibrillar Mineralization of Type I Collagen with Intermediate Precursors loaded Mesoporous Carriers. Sci Rep. 2015; 5:11199.
16. Boskey AL. Biomineralization: an overview. Connect Tissue Res. 2003; 44(Suppl 1):5–9.
17. Sodek J, Ganss B, McKee MD. Osteopontin. Crit Rev Oral Biol Med. 2000; 11(3):279–303.
18. Veis, A. Biomineralization. In: Simkiss, Kenneth, Wilbur, Karl M., editors. Cell Biology and Mineral Deposition. Vol. xiv. Academic Press; San Diego, CA: 1989. p. 337illus. $69.95; On BlomineralizationHeinz, A. Lowenstam and Stephen Weiner. Vol. x. Oxford University Press; New York: 1989. p. 324illus. $57Science. 1990; 247(4946):1129–30.
19. Fisher LW, Whitson SW, Avioli LV, Termine JD. Matrix sialoprotein of developing bone. J Biol Chem. 1983; 258(20):12723–7.
20. Bhattacharyya R, Chakrabarti P. Stereospecific interactions of proline residues in protein structures and complexes. J Mol Biol. 2003; 331(4):925–40.
21. Brandl M, Weiss MS, Jabs A, Suhnel J, Hilgenfeld R. C-H…pi interactions in proteins. J Mol Biol. 2001; 307(1):357–77.
22. Kar K, Ibrar S, Nanda V, Getz TM, Kunapuli SP, Brodsky B. Aromatic interactions promote self-association of collagen triple helical peptides to higher order structures. Biochem. 2009; 48(33): 7959–68.
23. Steiner T, Koellner G. Hydrogen bonds with pi acceptors in proteins: frequencies and role in stabilizing local 3D structures. J Mol Biol. 2001; 305(3):535–57.
24. Nam KT, Shelby SA, Choi PH, Marciel AB, Chen R, Tan L, Chu TK, Mesch RA, Lee BC, Connolly MD, Kisielowski C, Zuckermann RN. Free-floating ultrathin two-dimensional crystals from sequence specific peptoid polymers. Nat Mater. 2010; 9(5):454–60.
25. Sun J, Zuckermann RN. Peptoid polymers: a highly designable bioinspired material. ACS Nano. 2013; 7(6):4715–32.
26. Rosales AM, Segalman RA, Zuckermann RN. Polypeptoids: a model system to study the effect of monomer sequence on polymer properties and self-assembly. Soft Matter. 2013; 9(35):8400–8414.
27. Fowler SA, Blackwell HE. Structure function relationships in peptoids: recent advances toward deciphering the structural requirements for biological function. Org Biomol Chem. 2009; 7(8): 1508–24.

28. Seo J, Ren G, Liu H, Miao Z, Park M, Wang Y, Miller TM, Barron AE, Cheng Z. In vivo biodistribution and small animal PET of (64)Cu-labeled antimicrobial peptoids. Bioconjug Chem. 2012; 23(5):1069–79.
29. Zuckermann RN, Kodadek T. Peptoids as potential therapeutics. Curr Opin Mol Ther. 2009; 11(3): 299–307.
30. Chen CL, Qi J, Tao J, Zuckermann RN, DeYoreo JJ. Tuning calcite morphology and growth acceleration by a rational design of highly stable protein-mimetics. Sci Rep. 2014; 4:6266.
31. Chen CL, Qi J, Zuckermann RN, DeYoreo JJ. Engineered biomimetic polymers as tunable agents for controlling CaCO3 mineralization. J Am Chem Soc. 2011; 133(14):5214–7.
32. Olivier GK, Cho A, Sanii B, Connolly MD, Tran H, Zuckermann RN. Antibody mimetic peptoid nanosheets for molecular recognition. ACS Nano. 2013; 7(10):9276–86.
33. Zuckermann RN, Kerr JM, Kent SBH, Moos WH. Efficient method for the preparation of peptoids [oligo(N-substituted glycines)] by submonomer solid phase synthesis. J Am Chem Soc. 1992; 114(26):10646–10647.
34. Morrison JS, Nophsker MJ, Haskell RJ. A combination turbidity and supernatant microplate assay to rank-order the supersaturation limits of early drug candidates. J Pharm Sci. 2014; 103(10): 3022–32.
35. Clais S, Boulet G, Van Kerckhoven M, Lanckacker E, Delputte P, Maes L, Cos P. Comparison of viable plate count, turbidity measurement and real time PCR for quantification of Porphyromonas gingivalis. Lett Appl Microbiol. 2015; 60(1):79–84.
36. Krause S, Scholz T, Temmler U, Losche W. Monitoring the effects of platelet glycoprotein IIb/IIIa antagonists with a microtiter plate method for detection of platelet aggregation. Platelets. 2001; 12(7):423–30.
37. O'Leary MA, Maduwage K, Isbister GK. Use of immunoturbidimetry to detect venom antivenom binding using snake venoms. J Pharmacol Toxicol Methods. 2013; 67(3):177–81.
38. Reese SP, Underwood CJ, Weiss JA. Effects of decorin proteoglycan on fibrillogenesis, ultrastructure, and mechanics of type I collagen gels. Matrix Biol. 2013; 32(7–8):414–23.
39. Burwell AK, Thula Mata T, Gower LB, Habelitz S, Kurylo M, Ho SP, Chien YC, Cheng J, Cheng NF, Gansky SA, Marshall SJ, Marshall GW. Functional remineralization of dentin lesions using polymer-induced liquid precursor process. PLoS One. 2012; 7(6):e38852.
40. Chien YC, Burwell AK, Saeki K, Fernandez-Martinez A, Pugach MK, Nonomura G, Habelitz S, Ho SP, Rapozo-Hilo M, Featherstone JD, Marshall SJ, Marshall GW. Distinct decalcification process of dentin by different cariogenic organic acids: Kinetics, ultrastructure and mechanical properties. Arch Oral Biol. 2016; 63:93–105.
41. White JM, Goodis HE, Marshall SJ, Marshall GW. Sterilization of teeth by gamma radiation. J Dent Res. 1994; 73(9):1560–7.
42. McIntyre JM, Featherstone JD, Fu J. Studies of dental root surface caries. 1: Comparison of natural and artificial root caries lesions. Aust Dent J. 2000; 45(1):24–30.
43. Giraud Guille MM, Mosser G, Belamie E. Liquid crystallinity in collagen systems in vitro and in vivo. Curr Opin Colloid Interface Sci. 2008; 13(4):303–313.
44. Gobeaux F, Mosser G, Anglo A, Panine P, Davidson P, Giraud-Guille MM, Belamie E. Fibrillogenesis in dense collagen solutions: a physicochemical study. J Mol Biol. 2008; 376(5): 1509–22.
45. Kirkwood JE, Fuller GG. Liquid crystalline collagen: a self-assembled morphology for the orientation of mammalian cells. Langmuir. 2009; 25(5):3200–6.
46. Marshall GW, Habelitz S, Gallagher R, Balooch M, Balooch G, Marshall SJ. Nanomechanical properties of hydrated carious human dentin. J Dent Res. 2001; 80(8):1768–71.
47. Balooch M, Wu Magidi IC, Balazs A, Lundkvist AS, Marshall SJ, Marshall GW, Siekhaus WJ, Kinney JH. Viscoelastic properties of demineralized human dentin measured in water with atomic force microscope (AFM)-based indentation. J Biomed Mater Res. 1998; 40(4):539–44.
48. Oliver WC, Pharr GM. An improved technique for determining hardness and elastic modulus using load and displacement sensing indentation experiments. J Mat Res. 2011; 7(6):1564–1583.
49. Cisneros DA, Hung C, Franz CM, Muller DJ. Observing growth steps of collagen self-assembly by time-lapse high resolution atomic force microscopy. J Struct Biol. 2006; 154(3):232–45.

50. Narayanan B, Gilmer GH, Tao J, De Yoreo JJ, Ciobanu CV. Self-assembly of collagen on flat surfaces: the interplay of collagen-collagen and collagen-substrate interactions. Langmuir. 2014; 30(5):1343–50.

51. Habraken WJ, Tao J, Brylka LJ, Friedrich H, Bertinetti L, Schenk AS, Verch A, Dmitrovic V, Bomans PH, Frederik PM, Laven J, van der Schoot P, Aichmayer B, de With G, DeYoreo JJ, Sommerdijk NA. Ion association complexes unite classical and non-classical theories for the biomimetic nucleation of calcium phosphate. Nat Commun. 2013; 4:1507.

52. Li Y, Thula TT, Jee S, Perkins SL, Aparicio C, Douglas EP, Gower LB. Biomimetic mineralization of woven bone-like nanocomposites: role of collagen cross-links. Biomacromolecules. 2012; 13(1):49–59.

53. Kinney JH, Balooch M, Marshall GW, Marshall SJ. A micromechanics model of the elastic properties of human dentine. Arch Oral Biol. 1999; 44(10):813–22.

54. Kinney JH, Balooch M, Marshall SJ, Marshall GW Jr, Weihs TP. Atomic force microscope measurements of the hardness and elasticity of peritubular and intertubular human dentin. J Biomech Eng. 1996; 118(1):133–5.

55. Kinney JH, Balooch M, Marshall SJ, Marshall GW Jr, Weihs TP. Hardness and Young's modulus of human peritubular and intertubular dentine. Arch Oral Biol. 1996; 41(1):9–13.

56. Jin H, Jiao F, Daily MD, Chen Y, Yan F, Ding YH, Zhang X, Robertson EJ, Baer MD, Chen CL. Highly stable and self-repairing membrane mimetic 2D nanomaterials assembled from lipid like peptoids. Nat Commun. 2016; 7:12252.

57. Elhadj S, De Yoreo JJ, Hoyer JR, Dove PM. Role of molecular charge and hydrophilicity in regulating the kinetics of crystal growth. Proc Natl Acad Sci. 2006; 103(51):19237–42.

58. Fu G, Valiyaveettil S, Wopenka B, Morse DE. CaCO3 biomineralization: acidic 8-kDa proteins isolated from aragonitic abalone shell nacre can specifically modify calcite crystal morphology. Biomacromolecules. 2005; 6(3):1289–98.

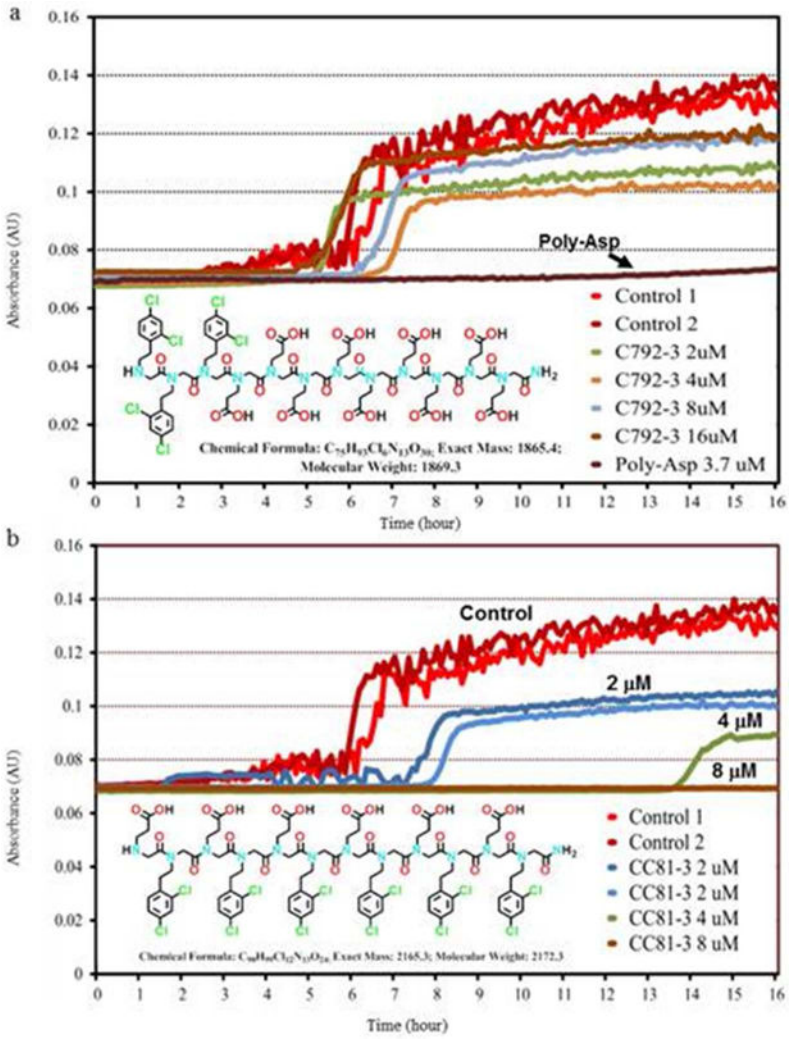

Figure 1.

Turbidity measurements showing the incubation time for nucleation of calcium phosphate from aqueous solutions ($[Ca^{2+}]$ = 6.75 mM, $[HPO_4^{2-}]$ = 3.15 mM in tris buffer at 37°C with NaN_3 added as a biocide). a) the addition of peptoid C792-3 at the concentrations shown. The results are compared to the turbidity data for peptoid-free solutions (Control), and solutions containing 3.7μM of 27 kDa pAsp. b) Inhibitory peptoid CC81-3, which delayed (blue and green curves, 2 and 4 μM, respectively) and completely inhibited (brown curve, 8 μM) nucleation of calcium phosphates

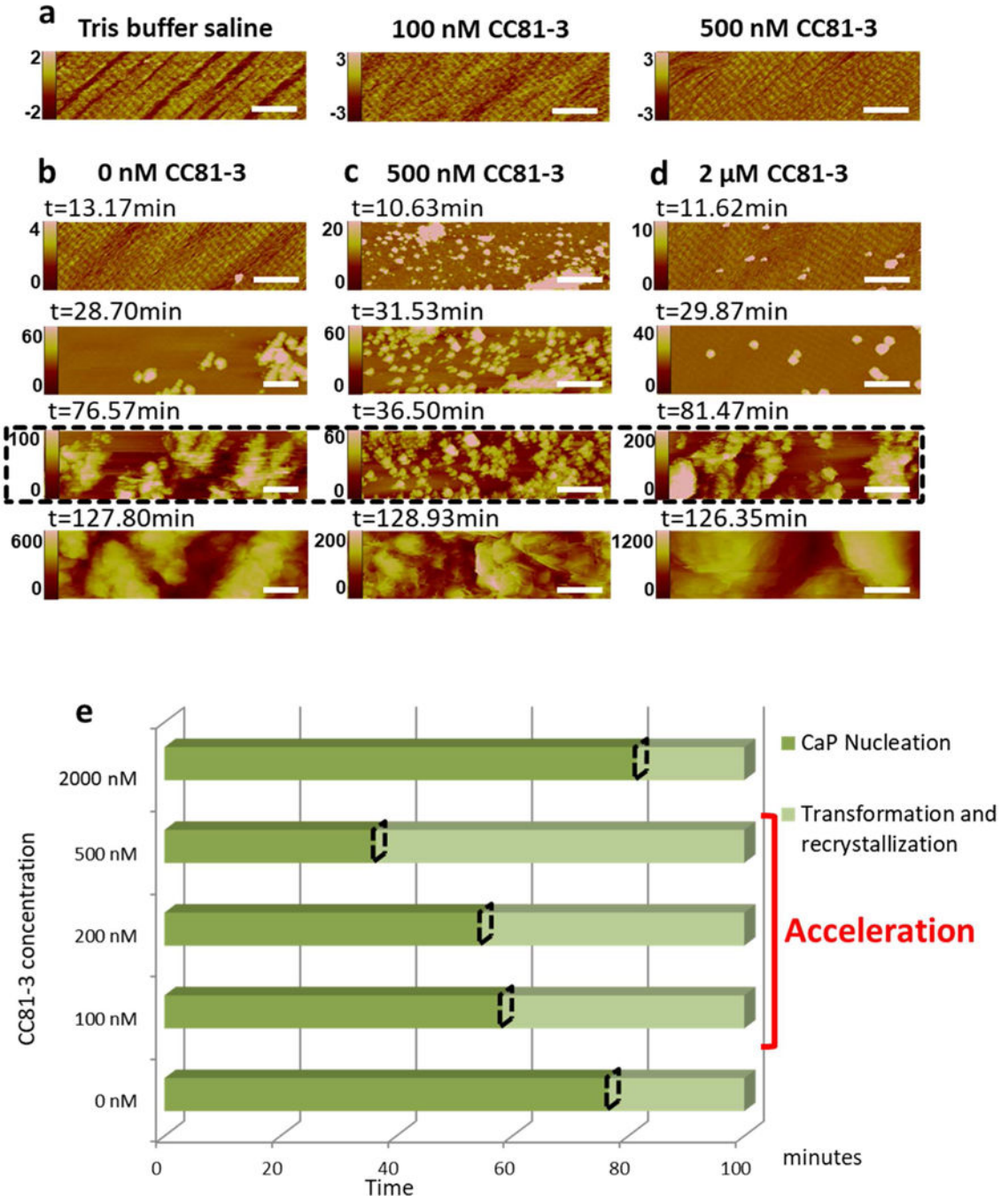

Figure 2.

In situ AFM observations of peptoid influenced mineralization on pure collagen substrates assembled on mica in Tris buffer saline containing various concentrations of peptoid CC81-3. a) Collagen morphology and order following addition of peptoid solution. b–d) Time series showing amorphous calcium phosphate nucleation and crystallization on the collagen substrates shown in (a), during mineralization in calcium phosphate solution ($[Ca^{2+}]$ = 6.75 mM, $[HPO_4^{2-}]$ = 3.15 mM in tris buffer; σ=3.34) in the presence of peptoid CC81-3 at (b) 0, (c) 100 and (d) 500 nM. The images highlighted in dashed box (third row

of b–d) were collected at the time points when the phase transformation began. (e): Incubation time for amorphous calcium phosphate nucleation (dark green) and phase transformation (light green) from the results shown in (b–d). The onset time of the phase transformation is marked with a dashed rhombus. All scale bars are 500nm. The vertical scales for all AFM images are in nm.

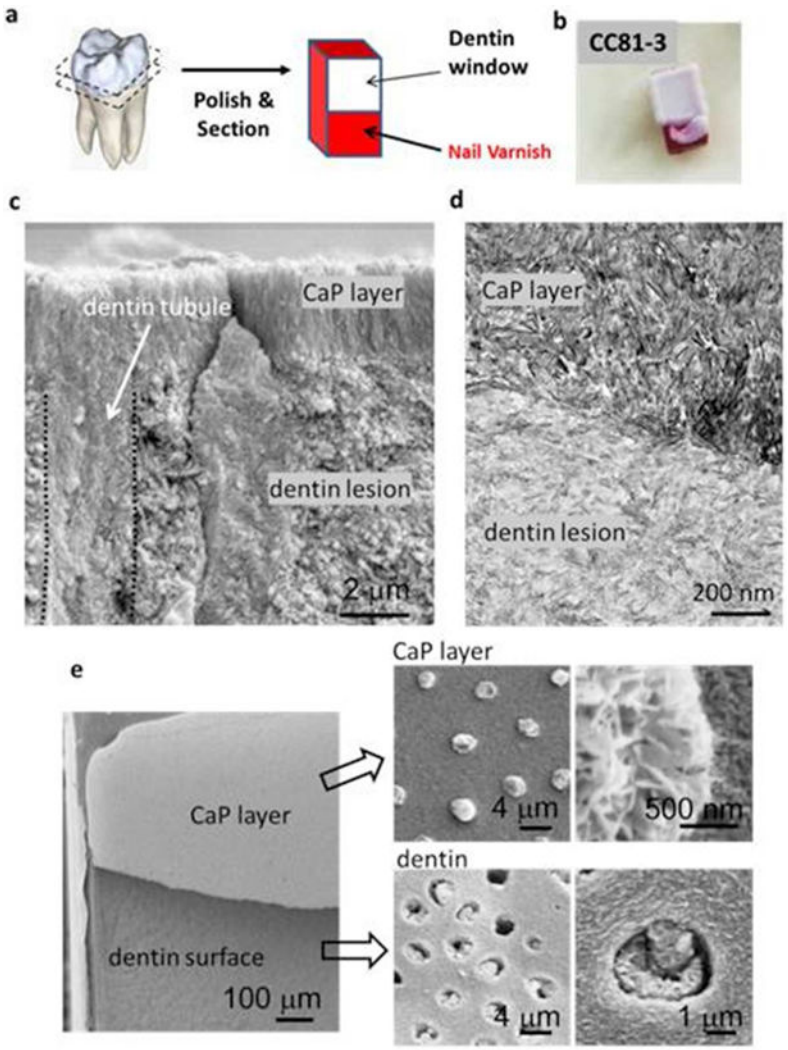

Figure 3.

Mineral layers formed on artificial dentin lesions from aqueous calcium phosphate solution (40 ml of peptoid-free solution at 37°C with $[Ca^{2+}] = 4.5$ mM, $[HPO_4^{2-}] = 2.1$ mM in tris buffer with NaN_3 added as a biocide) following incubation of the dentin block in solution containing peptoid CC81-3 (30 µl of 2 mM CC81 3 solution until dry). a) Artificial lesion window created in non-carious human dentin blocks with acid resistant nail varnish to simulate an occlusal natural carious lesion in a fissure that spreads laterally and into the dentin when it reaches the dentino-enamel junction (DEJ). b) Layer of calcium phosphate mineral formed exclusively on the top of dentin lesion using the protocol in (a). This mineral layer is firmly attached to the dentin lesion window. c) SEM image of fracture surface. Dentin tubules were also filled with calcium phosphate mineral (delineated by dotted lines). d) TEM image of ultrathin section. e) SEM of fractured interface between dentin surface and the calcium phosphate layer on the dentin surface and within the lumen of the dentin tubules (indicated by black arrows, with enlarged views at the right side).

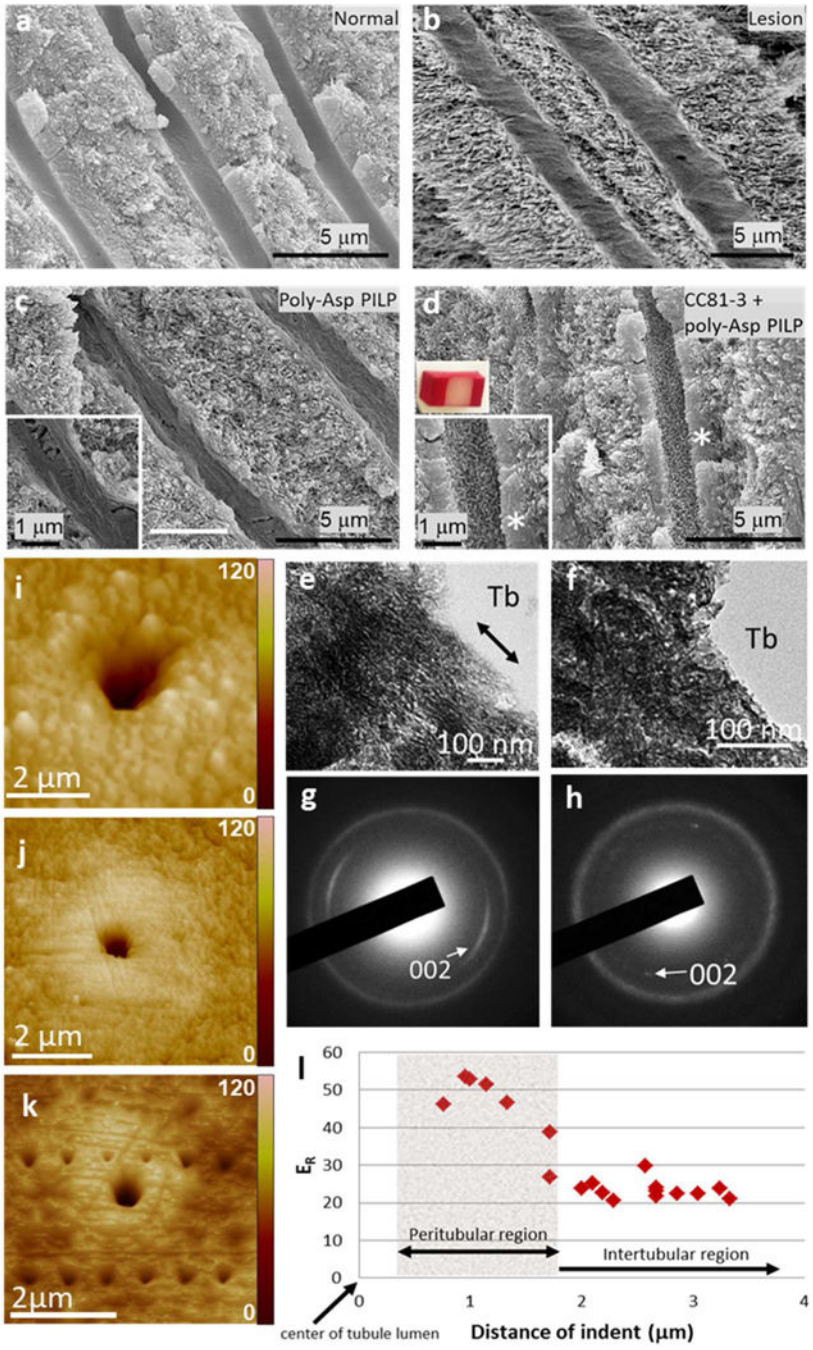

Figure 4.

Peptoid induced peritubular mineralization and change in mechanical properties. a–d) SEM images of (a) normal dentin, (b) artificial dentin lesions, (c) lesion remineralized via PILP process (40 ml of solution at 37°C with $[Ca^{2+}]$ = 4.5 mM, $[HPO_4^{2-}]$ = 2.1 mM in tris buffer with NaN_3 added as a biocide) and (d) via PILP process with pre-incubation in peptoid CC81-3 solution (2 μM peptoid and 100 μg/ml 27 kDa pAsp for 5 days). The addition of the incubation step with peptoid CC81-3 induced the peritubular mineralization (compare insets in (c) and (d)), resembling normal peritubular dentin. (e, f) TEM images with SAED data (g,

h) showing (e, g) peritubular minerals generated with addition of peptoid CC81-3 compared with (f, h) normal peritubular dentin. Tb: dentin tubule. Peptoid induced peritubular minerals consist of stack and co-aligned apatite nano-crystals (double head arrow guiding the view of alignment). i–k) AFM images showing peritubular remineralization. (i) Dentin tubule prior to remineralization (j) Dentin tubules 30–50% occluded by peritubular mineralization when the dentin lesion was incubated with 2μM peptoid prior to PILP remineralization. (k) Series of nano-indentations made across the occlusal surface of a remineralized dentin lesion in both the peritubular region and the intertubular region following peptoid-induced remineralization. l) Reduced elastic modulus (E_R) determined from the nano-indentations in (k). Values within the peptoid-induced peritubular mineral ranges from 40–55 GPa, which are markedly higher than the values measured either across the intertubular region or in normal peritubular dentin (28.6 GPa[53]). AFM image shows triangular indents across the occlusal surface of a remineralized dentin lesion using peptoid+PILP process. The vertical scales of all AFM images are in nm (i – k).

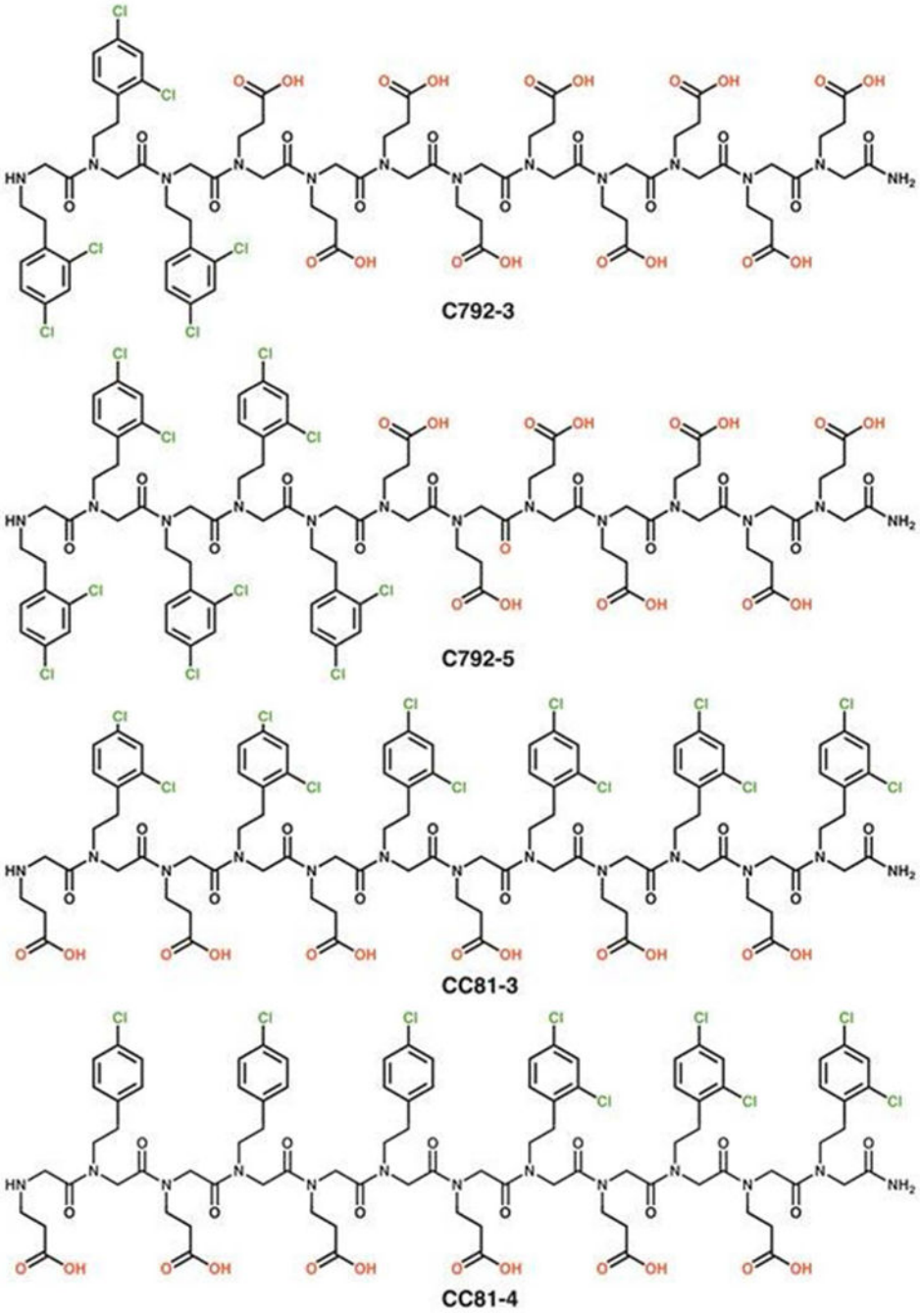

Scheme 1.
Structure of selected peptoid constructs.